Aerosol Science and Technology

ISSN: 0278-6826 (Print) 1521-7388 (Online) Journal homepage: https://www.tandfonline.com/loi/uast20

Size and Morphology of Soot Particulates Sampled from a Turbulent Nonpremixed Acetylene Flame

Bing Hu & Umit Koylu

To cite this article: Bing Hu & Umit Koylu (2004) Size and Morphology of Soot Particulates Sampled from a Turbulent Nonpremixed Acetylene Flame, Aerosol Science and Technology, 38:10, 1009-1018, DOI: 10.1080/027868290519111

To link to this article: https://doi.org/10.1080/027868290519111

Published online: 04 Mar 2011.

Aerosol Science and Technology, 38:1009–1018, 2004

ISSN: 0278-6826 print / 1521-7388 online
DOI: 10.1080/027868290519111

Size and Morphology of Soot Particulates Sampled from a Turbulent Nonpremixed Acetylene Flame

Bing Hu and Umit O. Koylu
Department of Mechanical and Aerospace Engineering, University of Missouri—Rolla, Rolla, Missouri

Soot processes within a turbulent nonpremixed flame burning acetylene/air were investigated by conducting thermophoretic sampling experiments at various axial and radial locations. Analyses of transmission electron microscope images yielded the mean soot spherule diameter, number of spherules per aggregate, and fractal morphology within this highly luminous turbulent flame. Specifically, translucent particles were observed at low-to-intermediate heights above the flame with the formation and evolution of young soot precursors. The soot spherule diameter peaked at 34 nm halfway along the centerline, identifying the flame regions of surface growth and oxidation processes. In the meantime, the aggregation was continuous along the flame axis with the mean number of spherules per aggregate reaching 150 at the highest sampling location. Size ranges of spherules and aggregates were narrow and broad, respectively, while the relative widths of both size distributions remained similar throughout the flame. In contrast to the observed axial variations, the radial changes of the mean spherule and aggregate sizes appeared to be small. Aggregate morphologies were universally characterized by a fractal dimension of 1.82 and a fractal prefactor of 1.9 for all the flame positions. In comparison to a lightly sooting ethylene flame, these measurements in the acetylene turbulent flame revealed that the fuel type mainly affected the axial evolution of spherule diameters but not their range, and enhanced the aggregate sizes but not their morphology. The effective decoupling of spherule and aggregate sizes permitted the separation of soot surface growth and oxidation from aggregation. This key aspect provided a stringent test for the existing particulate diagnostics and predictive models in their ability to quantify the actual particle surface area, particularly in optically thick conditions that are encountered in many practical combustion environments.

INTRODUCTION

The negative impact of submicron aerosols on human health and environment triggered new interest in soot particles that are generally produced during the incomplete combustion of fossil fuels. Satisfying stricter emission regulations is of special concern, especially for the transportation vehicles (e.g., diesel engines), which significantly contribute to the local air pollution levels. A major challenge for engine designers is the effective control of fine particulate matter without compromising other undesirable pollutants and thermal efficiency. The technology for resolving this demanding problem can be advanced by a comprehensive understanding and modeling of the soot formation and destruction mechanisms at conditions representative of practical combustors. Achieving this ultimate goal heavily depends on reliable measurements performed within controlled flame environments, which can offer convenient isolation of soot phenomena from other complications.

Current predictive models and emission standards have mainly been developed on the basis of particle mass. The key role of particle size has recently been emphasized due to the fact that particle surface area increases with decreasing size for a fixed mass. In particular, nanometer-size soot particles have tremendous active specific surface areas, resulting in enhanced chemical interactions with the surrounding flame. Accordingly, in situ (e.g., light scattering/extinction, laser-induced incandescence) and ex situ (e.g., thermophoretic sampling, differential mobility analyzer) diagnostics commonly have been utilized for measuring particle size and/or concentration. Noting the inherent difficulties associated with any experimental method in particulate-laden flames, these instruments provide independent information on physical soot properties with their respective advantages and disadvantages.

One of the most important considerations for the accurate characterization of particle size is to account for the actual micromorphology during the data interpretation. Specifically, spherical particles (spherules) collect into grapelike clusters (aggregates) in combusting flows because carbonaceous soot particles do not usually coalesce upon coagulation. As soot particles are convected up in a typical flame, the spherule diameter first increases due to the surface growth mechanism and then decreases due to the particle oxidation, depending on the local temperature and oxidizing species. In the meantime, the number of spherules

Received 8 March 2004; accepted 2 August 2004.
This research was sponsored by National Science Foundation (Grant No. CTS-0196012) and University of Missouri Research Board.
Address correspondence to Umit O. Koylu, Department of Mechanical and Aerospace Engineering, University of Missouri—Rolla, 1870 Miner Circle, 203 ME Building, Rolla, MO 65409-0050, USA. E-mail: koyluu@umr.edu

per aggregate mainly increases due to the unavoidable aggregation process. Hence, decoupling of spherule and aggregate sizes during the analysis of particulate diagnostics is essential for distinguishing these different soot processes. An overall dimension such as equivalent or mobility diameter combines the sizes of clusters and individual particles, resulting in the overestimation and underestimation of growth and oxidation rates, respectively. Such measurement errors in the reactive surface area compromise not only the development of reliable particle models in the combustion source but also the assessment of the influence of airborne particulates on human health and air quality.

Soot-containing turbulent flames are of engineering interest because they resemble the flow conditions in automotive engines, gas turbines, industrial furnaces, and natural fires closer than the laminar ones. Accordingly, they have been investigated in spite of the experimental difficulties associated with the inherent flow fluctuations; see, for example, Kent and Bastin (1984), Kent and Honnery (1987), Gore and Faeth (1988), Mungal and O'Neil (1989), Coppale and Joyeux (1994), Kennedy (1997), and references cited therein. Nevertheless, the database on the actual soot properties within turbulent flames is relatively limited, mainly due to the above-discussed experimental shortcomings that were noticed by the classical scattering experiments of Magnussen (1974). Reasonable data on soot spherule diameters in turbulent flames were reported by Prado et al. (1976) by removing particles from kerosene and benzene flames with a water-cooled probe and collecting them on a filter. Rapid thermophoretic sampling (TS) technique has recently allowed ex situ measurements of the soot spherule and aggregate sizes/morphologies in flames by means of direct visualizations of transmission electron microscope (TEM) images. In addition to a broad range of laminar conditions (e.g., Megaridis and Dobbins 1989; Cai et al. 1993), this experimental technique was successfully implemented in the overfire region of a number of turbulent flames (Koylu and Faeth 1992) and within a turbulent combustor (Fang et al. 1998). The former study only considered emitted particles with negligible chemical reactions, while the latter study was restricted to five axial locations within a complex flame. Recently in this laboratory, Hu et al. (2003) also employed the TS/TEM technique to quantify the mean soot spherule and aggregate sizes and fractal morphology at the axis of a turbulent nonpremixed ethylene/air flame. Various soot processes were separately identified in this well-defined, lightly sooting turbulent flame, which was convenient for comparisons to computational predictions.

One of the main objectives of the present study was to broaden the database on the actual soot processes within turbulent nonpremixed flames by extending the experiments of Hu et al. (2003). The effect of fuel type on particulate formation in a turbulent flow was explored by considering a heavily sooting acetylene flame with a high Reynolds number. Spatially resolved TS/TEM measurements were conducted not only at various heights above the burner along the flame centerline but also at some radial locations. The relatively high particle concentrations produced by acetylene offered conditions that are usually encountered in many realistic combustion environments. For example, practical combustors operate at elevated pressures that drastically enhance soot nucleation because particle volume fraction is nearly proportional to the pressure. Moreover, such thick clouds of particles resemble the conditions observed in diesel engines and natural fires that are major sources of airborne particulate matter. The experimental results in the highly luminous flame considered here also provide a stringent test for validation of turbulent soot models, which can be used to develop effective strategies to control particulate formation in more complex combustion systems. Finally, the present study is valuable for the interpretation of in situ laser-based measurements that are anticipated to be problematic within optically thick particulate-laden environments. In particular, the separation of soot spherule diameter from aggregate size is vital to assess the proficiencies of other diagnostics such as laser scattering/extinction, laser-induced incandescence, and differential mobility analyzer to measure specific particle surface area.

EXPERIMENTAL METHODS

The following discussion is brief, as further details of the experimental methods can be found in Hu (2002).

Turbulent Flame Apparatus

The burner was a 230 mm long tube with an inside diameter of $D = 6$ mm, similar to the one used by Sivathanu and Gore (1991). Acetylene gas was vertically issued from the burner to the stationary air at standard conditions. The measured fuel flow rate resulted in the exit test conditions summarized in Table 1. An axisymmetric turbulent nonpremixed jet flame was naturally stabilized at the burner tip. Strong continuum radiation from soot particles was obvious, as can be seen in the visible appearance of high luminosity with a bright yellow color throughout the flame (Figure 1). The burner could be moved vertically and horizontally using a computer-controlled system in order to access the desired axial and radial flame locations. The burner assembly was surrounded by plastic strips in a large enclosure that had an exhaust system at the top to discharge the combustion products. This simple, unconfined, and reproducible turbulent flame configuration was essential to facilitate a focused investigation of soot formation.

Table 1
Test conditions at the burner exit

Burner diameter	$D = 6$ mm
Acetylene mass flow rate	$\dot{m} = 0.76$ g/s
Average fuel gas velocity	$V = 4\dot{m}/\pi D^2\rho = 23$ m/s
Reynolds number	$\mathrm{Re} = VD/\nu = 15{,}100$
Richardson number	$\mathrm{Ri} = gD/V^2 = 1.1 \times 10^{-4}$

$\rho = 1.16$ kg/m^3 and $\nu = 9.1 \times 10^{-6}$ m^2/s were used for the acetylene gas at standard conditions.

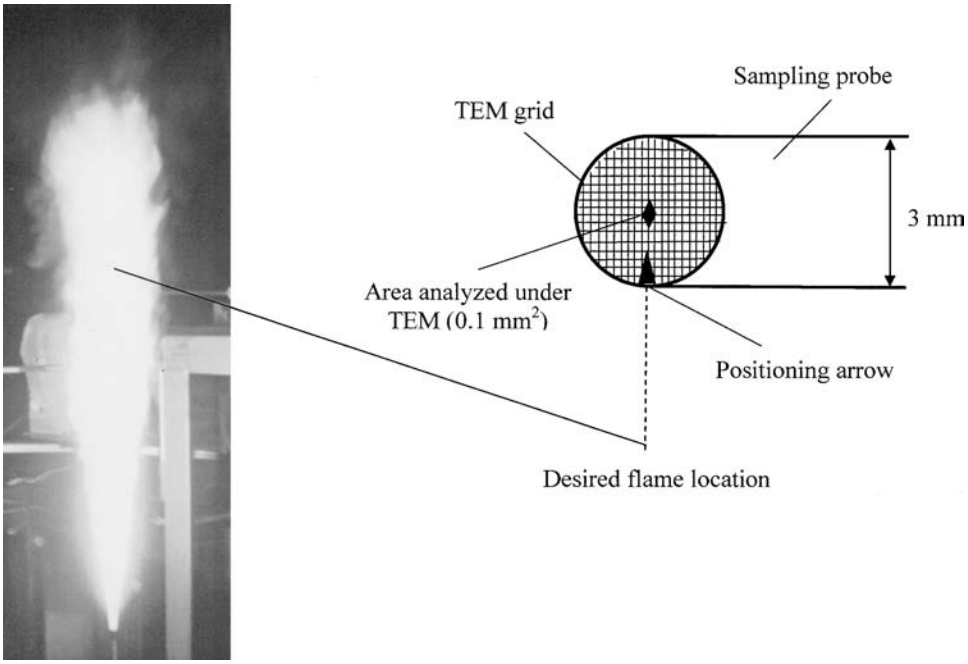

Figure 1. Still photograph of the turbulent nonpremixed acetylene flame and general features of the sampling grids.

Thermophoretic Sampling

The TS technique involves quick insertion of a sampling surface (TEM grid) attached to a small cold probe into a hot particle-laden environment and deposition of particles by thermophoresis due to the temperature difference across the boundary layer. Subsequent visual observation of the grid under a TEM provides images of representative particles whose size and morphology can be analyzed using computer image software. Although an intrusive method, TS has two key advantages over other sampling experiments: minimum flame intrusion with the completion of sampling in milliseconds and one-step extraction process with no sample manipulations. Furthermore, direct TEM characterization is independent of particle refractive index, density, and morphology in contrast to the optical diagnostics that require interpretations. Therefore, since first designed by Dobbins and Megaridis (1987), the TS technique has been successfully implemented in mainly laminar flames to offer data for not only advancing our knowledge on soot phenomena but also complementing in situ laser-based measurements.

The present sampling probe was a metal substrate of 0.5 mm thickness and 3.05 mm width, carrying a single TEM grid of 3 mm diameter at its tip for each sampling. As illustrated in Figure 1, the special copper grids had edge arrows for their orientation nearly parallel to the mean flow field. A positioning accuracy of less than 0.5 mm was achieved by first aligning a laser with the axisymmetric flame and then positioning the probe tip relative to the beam. When actuated by a double-acting air cylinder, the sampling probe extended to the desired flame location, slightly beyond a rectangular protective tube, which helped minimize the particle contamination before, during, and after sampling. The probe stayed in the flame for 15–40 ms so that less than 15% of the grid area was covered by nonoverlapping particles. This exposure time was long enough compared to the typical flow fluctuations of ca. 1–3 ms in this turbulent jet flame, so that the present measurements represented time-averaged soot properties.

Transmission Electron Microscope

After collecting soot populations at a flame location, a grid was taken to a Philips EM 430T TEM with a point-to-point resolution of 0.24 nm. An operating voltage of 100 kV was used to improve the contrast level between the particles and the carbon film supporting the TEM grids. Different magnifications in the range of 10,300–52,100 were typically considered during this study. The vertical arrow and diamond-shaped center markings on grids (Figure 1) allowed accurate correspondences between the desired flame locations and microscope coordinates. Randomly chosen particles were photographed only near the grid centers at a few meshes of approximately 0.1 mm^2, which was substantially smaller than the overall grid area. Consequently, the present TS experiments had a spatial resolution that was sufficient to resolve even the smallest soot streaks existing in turbulent flames.

Image Enhancement and Analysis

The TEM photographs were first digitized using a high-resolution scanner and then saved on a personal computer for analysis using advanced image software. The automatic computer detection of aggregates was convenient, yet it alone was inadequate to virtually eliminate some inherent imaging problems.

For example, TEM images generally suffer from partial poor contrasts due to the weak illuminations at relatively high magnifications. Random noise may also be present in the images due to the nonuniform illuminations and/or electron fluctuations. Furthermore, Fresnel phenomena can be caused by the electron diffraction at particle edges. Without visual human inspections, random noise could be recognized artificially as tiny particles by the computer, whereas bright edges could lead to the separation of an aggregate into smaller aggregates after intensity threshold. Various image enhancement methods discussed below were therefore utilized to improve the TEM images for a qualitative analysis.

First, stretching of the dynamic range of gray level transformed original images to the ones with the full intensity range of 0–255, increasing the contrast between the particles and the background. Low-pass filtering was then applied to exclude random noise without compromising the identification of particle edges. In particular, spatial convolution filters with different mask sizes were employed to attain an optimum between noise reduction and edge preservation. The appropriate filtering also blurred the bright edges, which were unfavorable for the subsequent threshold. Both global and manual threshold methods were considered to convert the grayscale images to binary ones containing only black particles on a white background. Although threshold process may occasionally result in a few broken aggregates, image closing (dilation combined with erosion) was found to be effective to resolve this potential problem by fusing and filling any isthmuses. Because this threshold stage mainly governs the accuracy of automatic computer measurements, several sizes of square structure elements were tested for optimal particle tracing on a trial-and-error basis with visual inspections. Finally, segmentation was employed to recognize and label each object in the image by automatically scanning the image pixel by pixel. By applying the same procedures of TEM photography, digitization, and computer image analysis to the known-size latex spheres, a calibration factor to convert the pixel scale on digitized images to the nanometer scale was obtained for each magnification used.

RESULTS AND DISCUSSION

General Observations

General appearances of soot sampled from the flame centerline at four different heights above the burner, z/D, are shown in the typical TEM photographs of Figure 2. An approximate scale of 100 nm was displayed in each image for convenient visual comparisons. Similar to the measurements of Fang et al. (1998) and Hu et al. (2003), soot in this turbulent flame was in the form of aggregates containing smaller primary particles (spherules). At a particular flame location, substantial variations in aggregate sizes and shapes were seen, indicating a polydisperse distribution and a complex geometry. In contrast, the primary particles were spherical, and their nanometer diameters did not appear to vary on a TEM image. This general morphology of aggregated soot particles was also consistent with the extensive reports in laminar flames.

A careful inspection of the TEM pictures in Figure 2 revealed that there were some single particles mainly at the low-to-intermediate flame locations ($z/D < 50$). In sharp contrast to the opaque mature aggregates, they appeared to be more transparent to the electron beam with diffuse boundaries. Such translucent particles have been extensively observed in laminar flames; see Dobbins (1997) and references cited therein. Similar young soot precursor particles were also captured in a turbulent ethylene flame in this laboratory (Hu et al. 2003). It has been suggested that such material indicates the evolution of soot particles from a liquid state to a solid form by dehydrogenation and carbonization reactions (Prado et al. 1976; Dobbins 1997). The existence of these early soot particles, although slowed down with the height above the present burner, might imply some new particle formation occurring until the middle of this turbulent flame. Furthermore, their absence toward the flame tip was possibly due to the completion of their carbonization before being released to the surroundings.

The spherule and aggregate size statistics, as well as the fractal dimensions and prefactors, were quantified in the next section. In addition to the familiar mature particles/aggregates, the translucent particles discussed above were also counted during the present TEM analysis in spite of higher experimental uncertainties in distinguishing their intensity levels from the carbon-supported grid background. All the measurements were found to be repeatable within the experimental uncertainties that will be addressed together with the results. Main sources of uncertainties were associated with the flame intrusion by the sampling probe, dependence of thermophoretic velocity on particle size/morphology (Eisner and Rosner 1985), analysis of finite number of particles/aggregates, above-mentioned image enhancement procedures, and translucent particles. The propagations of measurement errors to the calculated parameters were evaluated following the standard uncertainty analysis of Moffat (1982); please see Fang et al. (1998) and Hu (2002) for detailed considerations.

Axial Variation of Spherule Diameter Distribution

After enhancing the high-magnification grayscale TEM images, spherule diameters, d_p, were measured by manually detecting the apparent profiles of spherical particles near the aggregate edges. Because of the narrow distribution at a particular flame position, 20–40 spherules were sufficient to build a statistically significant data set for the mean, $\bar{d}_p$, and its standard deviation, σ_p. Experimental uncertainties associated with $\bar{d}_p$ values were estimated to be about 5% for typical carbonized particles.

Mean soot spherule diameters measured at various axial heights along the flame centerline are illustrated in the first part of Figure 3. The mean spherule diameter was 17 nm at the lowest sampling position ($z/D = 5$) of the present tests. Prompt formation of particles right above the burner was expected with the high sooting propensity of acetylene fuel. In this turbulent flame

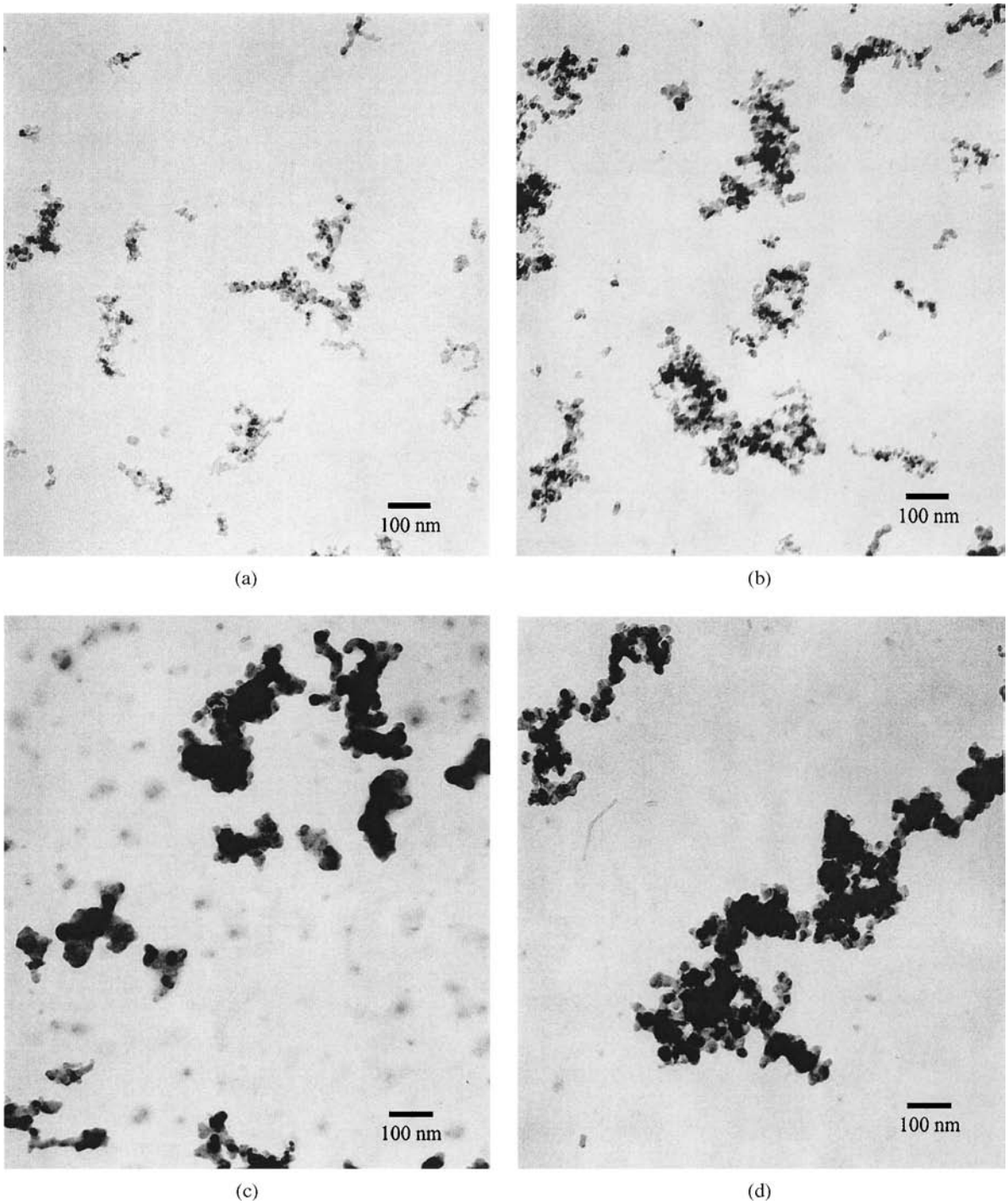

Figure 2. Typical TEM images of soot particulates at four heights above the burner along the flame centerline: (a) $z/D = 5$, (b) $z/D = 20$, (c) $z/D = 50$, and (d) $z/D = 80$.

$\bar{d}_p$ continued to increase until $z/D = 50$, reaching a maximum value of 34 nm due to the prevailing surface growth process. The mean spherule diameter then started decreasing slowly down to 27 nm until the highest sampling position of $z/D = 100$. Such consistently lower sizes after the peak axial location indicated the countereffect of particle oxidation in this region close to the flame tip. Standard deviations of spherule diameters, σ_p, are also demonstrated in the second part of Figure 3. They were 13–21% of the mean values and did not appear to change with the axial flame location. Such small $\sigma_p/\bar{d}_p$ ratios suggested a practical

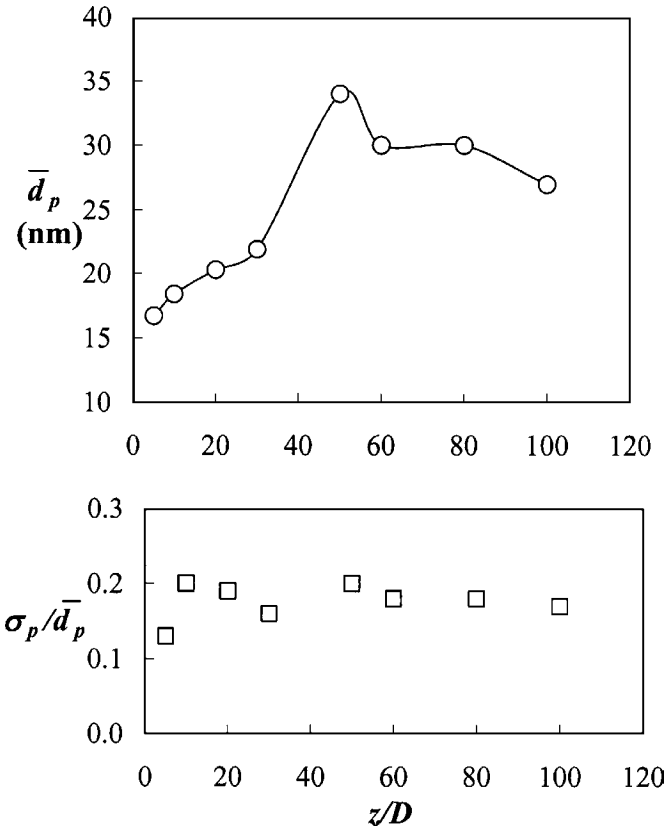

Figure 3. Axial variations of the mean and standard deviation of the spherule diameter distribution along the flame centerline.

representation of spherule size distribution with a Gaussian (normal) probability density function in turbulent flames.

The above size range of spherules is consistent with the previous studies in numerous laminar nonpremixed flames in which soot diameters are narrowly confined to 10–50 nm. This implies that the effect of turbulent flow field on the final spherule size is relatively minor. A pertinent comparison should also be made against the variations reported within other turbulent flames. The mean soot spherule diameters in an ethylene turbulent flame (Hu et al. 2003) were found to be 19–35 nm, which is nearly identical to the current range. In the meantime, the peak spherule size was encountered at a later height in the ethylene flame than the acetylene flame. These observations in two hydrocarbon flames indicate that the fuel type does not affect the spherule diameter range but its axial evolution. Therefore, the maximum soot loading in a flame appears mostly due to the nucleation mechanism forming more particles, whereas the effect of fuel structure appears to be important on the rates of surface growth and oxidation.

Two past studies independently reported soot spherule diameters within turbulent flames. Prado et al. (1976) considered the particle size distribution in two turbulent diffusion flames based on the electron microscope measurements, similar to the present study but only after extensive sampling manipulation (e.g., removal at the end of a probe with a filter and dispersion in an ultrasonic bath). Their mean spherule diameters of 19–30 nm and 18–22 nm at three locations in kerosene and benzene flames, respectively, are comparable to the present values. On the other hand, 10–13 nm spherule diameters measured by Fang et al. (1998) in a confined turbulent spray flame are a factor of 2–3 smaller than the values found in many combustion systems, including the turbulent flames in this laboratory. Fang et al. (1998) noted such lower size range and attributed it to the shorter residence times associated with a reaction stabilized by a swirl-induced recirculation zone. Although their $\sigma_p/\bar{d}_p$ ratios of 15–24% are in agreement with this study, the conveyed increase in $\sigma_p/\bar{d}_p$ with the burner height was in contrast to the present values, which did not exhibit a trend with the axial flame location. Additional studies could help resolve these discrepancies and determine the surface growth rates in turbulent flames.

Axial Variation of Aggregate Size Distribution

After intensity threshold of relatively low-magnification images, the projected areas, A_a, and maximum lengths, L, of aggregates were automatically measured with the computer software. The number of spherules in every aggregate within a binary-scale TEM image, N, was statistically estimated from

$$N = 1.15\left[\frac{A_a}{\pi \bar{d}_p^2/4}\right]^{1.09}. \qquad [1]$$

Equation (1) was a reasonable approximation to recover 3D aggregate properties from 2D projected images because it was not only in agreement with the computer simulations of cluster–cluster aggregates but also effective for the determination of aggregate sizes within turbulent flames (Fang et al. 1998; Hu et al. 2003). The constant 1.15 and the exponent 1.09 in Equation (1) approximately account for the overlapping of spherules. As demonstrated below, the aggregate morphological properties in the present turbulent flame are in excellent agreement with those in other types of flames, justifying the application of the above empirical correlation.

Reasonable population statistics were attained by acquiring 800–1000 random aggregates (including single particles) on a few meshes around the center of each grid carrying soot samples from a single flame position. Figure 4 displays the average number of spherules per aggregate, $\bar{N}$, at the flame axis as a function of the normalized height above the burner. The experimental uncertainty (95% confidence interval) in $\bar{N}$ was typically 40% as a result of the error propagation from the measured aggregate and spherule projected areas. As can be seen in the figure, $\bar{N}$ increased from about 30 to 150 between the lowest and highest sampling positions of $z/D = 5$ and 100. As expected, soot aggregates became continuously larger as they moved downstream along the flame centerline with the availability of more residence time for the unavoidable agglomeration process. Compared to the turbulent flames of Fang et al. (1998) and Hu et al. (2003), the acetylene flame produced aggregates about three

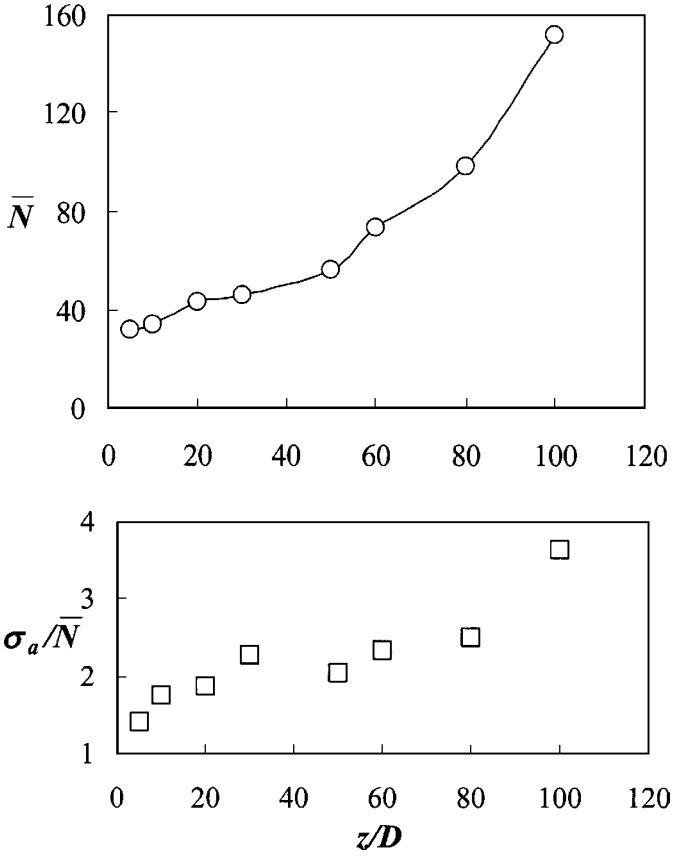

Figure 4. Axial variations of the mean and standard deviation of the aggregate size distribution along the flame centerline.

times bigger, mainly due to the enhanced aggregation associated with relatively higher particle concentration.

Although the determination of N from Equation (1) appears to depend on d_p, the ratio of aggregate and spherule projected areas only acknowledges the fact that the larger the spherule diameter the larger the aggregate size for the same number of spherules in an aggregate. Regardless, the spherule diameters were directly measured during the present experiments, independent of the aggregate size. This effective decoupling of spherule diameter from aggregate size in the TEM analysis was essential for accurate descriptions of soot aerosol dynamics in turbulent flames because it allowed separation of the soot surface growth and oxidation processes from the aggregation process. A comparison of Figures 3 and 4 reveals that the surface growth and oxidation dominate before and after $z/D = 50$, respectively, while the aggregation prevails throughout both flame regions. In other words, the surface growth and aggregation mechanisms were parallel to each other in the first half of the flame, making the overall soot size larger. The spherules gradually shrank higher in the flame where the oxidation and aggregation mechanisms worked, this time in the opposite directions for the overall soot size. Combining $\bar{d}_p$ and $\bar{N}$ in a single size parameter could therefore lead to the overestimation of soot surface growth rate early in a flame and the underestimation of oxidation rate at upper flame portions.

In order to briefly demonstrate these potential errors, let us consider an overall particle size, say the volume-equivalent diameter defined as $\bar{D}_{eq} = \bar{N}^{1/3}\bar{d}_p$. The present values of $\bar{d}_p$ and $\bar{N}$ yielded a continuous increase in $\bar{D}_{eq}$ from 53 nm to 144 nm, which were about a factor of three larger than the spherule diameters. Accordingly, proportional errors in specific soot surface areas could be faced throughout the flame by employing an experimental characterization that improperly ignores the actual aggregated morphology. Moreover, the oxidation region would be mostly overlooked because the increase in aggregate size almost overwhelms the decrease in spherule diameter in the flame. This could offer an explanation as to why some past studies reported soot particle sizes increasing in oxidation regions of turbulent nonpremixed flames, e.g., Geitlinger et al. (1999) based on the spherical analysis of optical measurements.

Soot aggregate size distribution was also sought because of its importance in both the interpretation of optical experiments and the modeling of soot formation in turbulent flames. Typical aggregate size distributions within a wide range of combustion environments have been demonstrated in the past (Megaridis and Dobbins 1989; Koylu and Faeth 1992; Fang et al. 1998). As illustrated in the second part of Figure 4, the standard deviations, σ_a, of the number of spherules per aggregate were always more than the average values. Although the aggregate size distributions at the lowest and highest flame sampling locations were somewhat narrower or broader, the axial variation of $\sigma_a/\bar{N}$ ratio was relatively small between $z/D = 10$ and 80. An average value of 2.1 for $\sigma_a/\bar{N}$ ratio suggested a practical representation of the aggregate size distribution with either a log-normal or an exponential-scaling probability density function. In general, there was a modest agreement between the experimental and theoretical pdfs, with deviations noted for aggregates with less than 8 spherules. The change in the shape of aggregate size distribution with sampling position could not be noticed within the current experimental uncertainties.

Axial Variation of Aggregate Fractal Properties

Different shape and size aggregates observed on TEM photographs (Figure 2) were described by the fractal concept that links the aggregate mass to its characteristic length, i.e.,

$$N = k_f \left(\frac{2R_g}{d_p} \right)^{D_f}. \qquad [2]$$

In this statistical relationship, D_f is the fractal dimension and k_f is the fractal prefactor (lacunarity), and they are both necessary to fully characterize the cluster morphology. Because the aggregate radius of gyration, R_g, was not directly measurable from projected images, an alternative aggregate length in terms of L was used. For a typical flame height of $z/D = 30$, Figure 5 shows the existence of such a statistical relationship between N and L/d_p in the form of Equation (2) for aggregates with 2 to

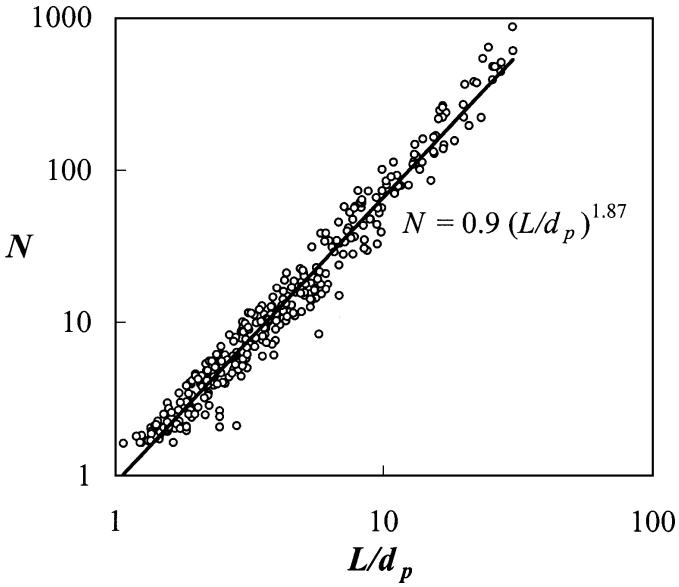

Figure 5. Determination of fractal properties from the statistical relationship between the aggregate mass and its characteristic length at a typical flame height.

1000 spherules. The linear least-square fit to such data at this flame position produced $D_f = 1.87$ from the slope and a correlation constant of $k_L = 0.9$, which was converted to $k_f = 1.8$ using

$$\frac{k_f}{k_L} = \left(\frac{D_f + 2}{D_f}\right)^{D_f/2}, \qquad [3]$$

The above equation was based on the experimental and theoretical investigations that captured the actual aggregate size, R_g, from the projected aggregate maximum length, L.

Repeating the above procedure for each sampling location, D_f and k_f values were determined along the flame centerline. As summarized in Figure 6, fractal dimensions were restricted to 1.77–1.88, whereas fractal prefactors were 1.6–2.2 without displaying any particular trend with respect to z/D. In fact, these axial variations were mostly within the experimental uncertainties, which were estimated to be about 5% for D_f and 30% for k_L (95% confidence intervals). Thus, fractal properties were generally invariable with the height above the burner in this turbulent flame.

The present range of $D_f = 1.82 \pm 0.06$ was in excellent agreement with past investigations in turbulent flames. Specifically, the aggregate fractal dimensions reported by Fang et al. (1998) were 1.80 ± 0.06. Although slightly lower D_f values of 1.74 ± 0.11 were found in a turbulent ethylene flame in this laboratory (Hu et al. 2003), the differences were still within experimental uncertainties and therefore considered to be statistically insignificant. Because these results in turbulent flames were also analogous to the numerous past investigations in laminar flames, soot fractal dimension appears to be remarkably insensitive to

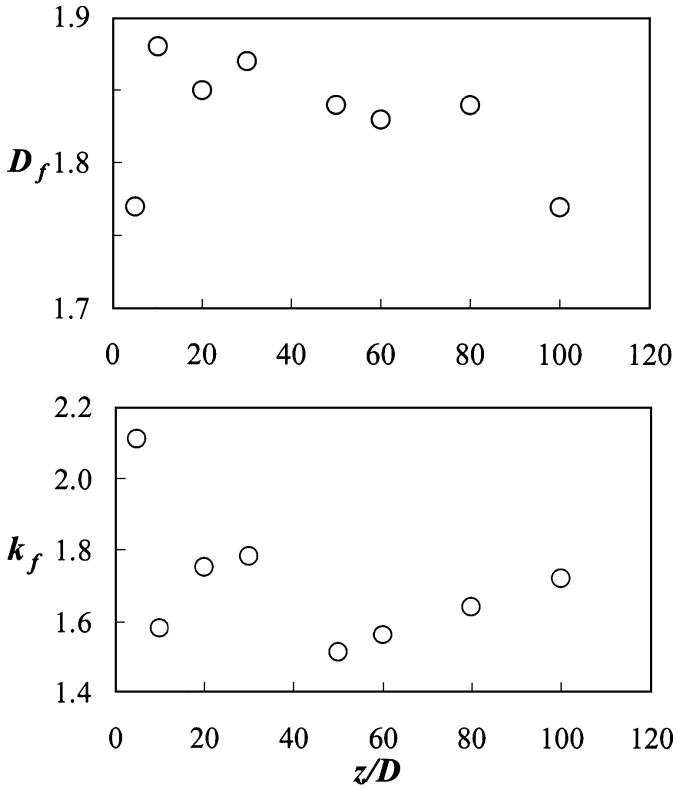

Figure 6. Axial variations of the aggregate fractal dimension and prefactor along the flame centerline.

flame location, flow condition, and fuel type. Numerical simulations validated this universal morphology as a consequence of the dominant diffusion-limited cluster-to-cluster agglomeration mechanism.

In contrast to the broad consensus on D_f in the literature, there are notable differences for the fractal prefactor, which varies between 1.2 and 3.4 among different studies. Some of this discrepancy may be due to the relatively large experimental uncertainties involved in estimating k_f with its high sensitivity to the fractal dimension (see Equation (3)). Nevertheless, the present prefactors of 1.9 ± 0.3 were still in reasonable agreement with the range of 2.2 ± 0.4 in a turbulent ethylene flame (Hu et al. 2003) within uncertainties. They were also comparable to the majority of experimental values in laminar flames. Note that this general accord between this and past experimental studies for the fractal morphology justified the adoptions of Equations (1)–(3) for the analysis of soot particulates in turbulent flames.

Radial Variations of Soot Properties

In addition to the above axial variations, radial changes of the soot properties were also measured during the present tests. Table 2 summarizes these TEM findings for three radial locations at two different heights above the burner. Not surprisingly, the fractal properties, D_f and k_f, did not vary with the radial flame position either. Evidently, radial variations of mean

Table 2
Radial variations of soot properties in the flame

z/D	r/D	d_p (nm)	$\bar{N}$	D_f	k_f
50	0	34	56	1.84	1.5
50	3	32	60	1.75	1.7
50	6	33	55	1.79	1.7
100	0	27	152	1.77	1.7
100	4	24	185	1.83	1.8
100	8	25	178	1.84	1.8

spherule and aggregate sizes were also relatively small. In fact, the differences in $\bar{d}_p$ and $\bar{N}$ from one radial location to another at both flame heights were within the cited experimental uncertainties. This striking observation may simplify the understanding of soot-containing turbulent nonpremixed flames. However, additional independent experiments considering a broader range of conditions should be considered to confirm this uniform radial behavior.

SUMMARY AND CONCLUSIONS

Motivated by the negative impact of submicron particles on human health and environment and the presence of turbulent conditions in many practical combustion systems, soot formation in a turbulent nonpremixed flame was experimentally investigated. A simple unconfined burner configuration was utilized to isolate soot processes within an axisymmetric jet flame burning acetylene in atmospheric-pressure air with relatively high Reynolds number. After rapid sampling of representative particles with a small thermophoretic probe, the mean soot properties were measured by direct visualizations and analyses of transmission electron microscope images. Distributions of soot spherule diameter and the number of spherules per aggregate as well as the aggregate fractal properties were quantified at various axial locations along the centerline and limited radial locations of the flame. The results were compared to two past studies in turbulent flames by Fang et al. (1998) burning liquid JP-4 fuel in a confined combustor and Hu et al. (2003) burning gaseous ethylene in a configuration similar to this study.

The general soot appearance was observed to be similar to those found in other combustion environments, that is, typically different shape and size aggregates consisting of nearly uniform-size spherical particles (spherules) at a fixed flame location. In particular, young soot precursor particles were observed at low-to-intermediate flame locations, similar to their existence in laminar flames. With their disappearance at upper flame positions, these translucent particles were evidently carbonized along the flame centerline. The mean spherule diameters were in the range 17–34 nm, peaking at a height of $z/D = 50$ and then gradually decreasing higher in the flame. This axial variation identified that the surface growth mechanism was dominant in the first half of the flame, with the oxidation process prevailing in the upper regions. Compared to the measurements in a lightly sooting ethylene flame in this laboratory, the present spherule size range was nearly identical with the maximum reached at an earlier height above the burner. This suggests that the effect of fuel type is mainly on the rate of axial change of spherule diameter but not its final range. The aggregate size in this heavily sooting acetylene flame always increased with the downstream location (residence time), denoting a continuous aggregation process along the centerline. As a result of the enhanced aggregation with higher particle concentrations, the mean number of spherules per aggregate reached 150, which is about three times larger than the ones produced in a lightly sooting ethylene flame. The ratios of standard deviations and averages for spherules and aggregates were approximately 0.18 and 2.1, respectively, with relatively minor changes in the flame, indicating a narrow distribution of spherules and a broad distribution of aggregates at each location. As expected from a cluster–cluster aggregation mechanism, the average fractal dimension and prefactor were 1.82 and 1.9, respectively, almost invariable throughout the flame. Interestingly, neither the mean spherule diameter nor the mean number of spherules per aggregate appeared to vary with radial flame location for the sampling conditions considered here.

The present experiments successfully decoupled soot spherule diameter from aggregate size, leading to the accurate characterization of particle surface area. Effective separation of the particle surface growth and oxidation processes from the continuous aggregation process was essential for a reliable understanding of soot aerosol dynamics in turbulent flames. Consequently, the findings reported here were valuable not only in advancing computational soot models but also assessing other particulate diagnostics. Moreover, the influence of fuel type on various soot mechanisms was explored by considering a heavily sooting acetylene flame, which broadened the limited database on the actual soot properties within turbulent nonpremixed flames. Such a highly luminous condition was relevant to many realistic combustors operating at elevated pressures, e.g., diesel engines, which substantially contribute to the particulate pollution in the atmosphere. The independent ex situ soot measurements also paved the way to the interpretation of in situ laser diagnostics, which should be implemented to investigate a wider range of experimental conditions, yet with anticipated challenges in optically thick turbulent flames.

REFERENCES

Cai, J., Lu, N., and Sorensen, C. M. (1993). Comparison of Size and Morphology of Soot Aggregates as Determined by Light Scattering and Electron Microscope Analysis, *Langmuir* 9:2861–2867.

Coppale, A., and Joyeux, D. (1994). Temperature and Soot Volume Fraction in Turbulent Diffusion Flames: Measurements of Mean and Fluctuating Values. *Combust. Flame* 96:275–285.

Dobbins, R. A., and Megaridis, C. M. (1987). Morphology of Flame-Generated Soot as Determined by Thermophoretic Sampling, *Langmuir* 3:254–259.

Dobbins, R. A. (1997). The Early Soot Formation in Hydrocarbon Flames. In *Physical and Chemical Aspects of Combustion*, Chap. 5, Gordon and Breach, Newark, NJ, pp. 107–133.

Eisner, A. D., and Rosner, D. E. (1985). Experimental Studies of Soot Particle Thermophoresis in Non-isothermal Combustion Gases Using Thermophoretic Response Techniques, *Combust. Flame* 61:153–166.

Fang, T. C., Megaridis, C. M., Sowa, W. A., and Samuelsen, G. S. (1998). Soot Morphology in a Liquid-Fueled, Swirl-Stabilized Combustor, *Combust. Flame* 112:312–328.

Geitlinger, H., Streibel, Th., Suntz, R., and Bockhorn, H. (1999). Statistical Analysis of Soot Volume Fractions, Particle Number Densities and Particle Radii in a Turbulent Diffusion Flame, *Combust. Sci. Technol.* 149:115–134.

Gore, J. P., and Faeth, G. M. (1988). Structure and Radiation Properties of Luminous Turbulent Acetylene/Air Diffusion Flames, *J. Heat Transf.* 110:173–181.

Hu, B. (2002). Thermophoretically-Sampled Soot Morphology at the Axes of Non-premixed Turbulent Jet Flames at Atmospheric Pressure, M.S. Thesis, University of Missouri–Rolla, Rolla, MO.

Hu, B., Yang, B., and Koylu, U. O. (2003). Soot Measurements at the Axis of an Ethylene/Air Non-premixed Turbulent Jet Flame, *Combust. Flame* 134:93–106.

Kennedy, I. M. (1997). Models of Soot Formation and Oxidation, *Prog. Ener. Combust. Sci.* 23:95–132.

Kent, J. H., and Bastin, S. J. (1984). Parametric Effects on Sooting in Turbulent Acetylene Diffusion Flames, *Combust. Flame* 56:29–42.

Kent, J. H., and Honnery, D. (1987). Soot and Mixture Fraction in Turbulent Diffusion Flames, *Combust. Sci. Technol.* 54:383–397.

Koylu, U. O., and Faeth, G. M. (1992). Structure of Overfire Soot in Buoyant Turbulent Diffusion Flames at Long Residence Times, *Combust. Flame* 89:140–156.

Magnussen, B. F. (1974). An Investigation into the Behavior of Soot in a Turbulent Free Jet C_2H_2-Flame, *Proc. Combust. Inst*. 15:1415–1425.

Megaridis, C. M., and Dobbins, R. A. (1989). Morphological Description of Flame-Generated Material, *Combust. Sci. Techol.* 71:95–109.

Moffat, R. J. (1982). Describing Uncertainties in Single-Sampling Experiments, *J. Fluids Eng.* 104:250–258.

Mungal, M. G., and O'Neil, J. M. (1989). Visual Observations of a Turbulent Diffusion Flame, *Combust. Flame* 78:377–389.

Prado, G. P., Lee, M. L., Hites, R. A., Hoult, D. P., and Howard, J. B. (1976). Soot and Hydrocarbon Formation in a Turbulent Diffusion Flame, *Proc. Combust. Inst.* 16:649–661.

Sivathanu, Y. R., and Gore, J. P. (1991). Simultaneous Multiline Emission Absorption Measurements in Optically Thick Turbulent Flames, *Combust. Sci. Technol*. 80:1–21.